


μ CT-Based Topography Analysis of Inaccessible Surfaces Exemplified by a Biofouling-Covered Plastic

Florian Bittner* and Hans-Josef Endres

DOI: 10.1002/cite.202100170

 This is an open access article under the terms of the Creative Commons Attribution-NonCommercial License, which permits use, distribution and reproduction in any medium, provided the original work is properly cited and is not used for commercial purposes.

Dedicated to Prof. Dr. rer. nat. Jürgen Caro on the occasion of his 70th birthday

The measurement of surface topographies is usually restricted to surfaces that are directly accessible to tactile or optical sensing. With this paper, the application of micro-computed tomography to measure characteristics of surfaces that are covered by solid films and thus not directly accessible is demonstrated. The method is first validated by comparative measurements of a plastic sample with μ CT and conventional optical profilometry. Afterwards, the μ CT-based method is successfully applied to a polyhydroxybutyrate plastic sample covered by biofouling after exposure to marine environment, providing insight into the degradation processes.

Keywords: Micro-computed tomography, Nondestructive testing, Plastic biodegradation, Surface roughness, Surface topography

Received: September 08, 2021; *revised:* October 15, 2021; *accepted:* November 18, 2021

1 Introduction

Surface topography of materials is of major importance for various chemical, physical, and biological processes, e.g., regarding catalytic activity, adsorption capacity, coating integrity, or corrosion behavior of materials. Typical methods to measure surface topography on different scales are based on atomic force microscopy or tactile and optical profilometry [1, 2]. All established methods have in common that they require direct accessibility of the surface to be measured. Surfaces that are inaccessible, e.g., because of geometric restrictions like inner surfaces of tubes or because of films present on the surfaces, cannot be measured or only with high preparatory effort and after destroying the sample or product.

In recent years, micro-computed tomography (μ CT) has become an established method in materials science for the nondestructive investigation of the internal structure and geometric properties of materials and components. The method is based on the transmission of X-rays through samples. From absorption images, taken from different rotation angles of the sample, a 3-dimensional volume is reconstructed, which reflects the local X-ray absorption for each contained voxel. In principle, every type of material can be investigated by μ CT, provided it can be penetrated by X-rays. Depending on system configuration and sample size, voxel resolutions down to the sub-micrometer range are possible. Typical applications include the analysis of

porosity, foam structure, or fiber orientation of materials [3, 4]. For industrial applications, also the dimensional metrology of components is of high importance. To obtain accurate results, various algorithms for surface determination were developed [5]. CT-based surface determination can also be used to analyze the surface topography of materials. This was reported in the past with a focus on additively manufactured samples [6–10]. In comparison to standard methods, advantages were reported for the μ CT method when analyzing high-roughness surfaces. For low-roughness surfaces, limitations can arise, depending on spatial resolution and image noise [6]. The surface roughness of an internal surface, in this case a maraging steel cooling channel produced by selective laser melting, was already successfully analyzed by Klingaa et al. [7].

As an example of the importance of being able to describe surface characteristics in applied material sciences, the biodegradation of plastics in a marine environment will be introduced briefly. The ubiquitous presence of plastic particles is recognized as a potential threat to diverse ecosystems, especially marine ecosystems [11]. However, the

Dr. Florian Bittner, Prof. Dr.-Ing. Hans-Josef Endres
bittner@ikk.uni-hannover.de
Leibniz University Hannover, Institute of Plastics and Circular Economy IKK, An der Universität 2, 30823 Garbsen, Germany.

knowledge about the persistence of plastics in the oceans is still limited [12]. The degradation of polymers can occur by various mechanisms, including photodegradation, thermooxidative degradation, mechanical degradation, or biodegradation. The latter mechanism, driven by biological systems, is particularly important for biodegradable plastics [13, 14]. One challenge to understanding degradation mechanisms and rates is the large number of abiotic and biotic environmental factors combined with specific material properties that influence degradation [13, 15].

Depending on the degradation mechanism, surface erosion or bulk erosion dominates. Consequently, for materials degrading predominantly via surface erosion, the surface area is an important factor for the rate of degradation [14–16]. Therefore, it is important to be able to track the change in surface parameters such as roughness and specific surface area, especially when considering thick-walled plastic items with an originally low surface-to-volume ratio. Field tests allow the exposure of macroscopic plastic samples to realistic environmental conditions. Frequently the exposed samples are covered by massive biofouling, as seen in Fig. 1a. Their removal can damage the samples or at least their surface as the subject of investigation and thereby falsify results. Therefore, for investigating the degradation of plastics in marine environment, μ CT is considered a valuable method. The nondestructive analysis allows not only to determine the degree of disintegration but also to characterize the surface topography of the plastic covered by the biofouling. This can be used to investigate correlations between initial surface roughness, formation of biofouling, and progression of plastic disintegration.

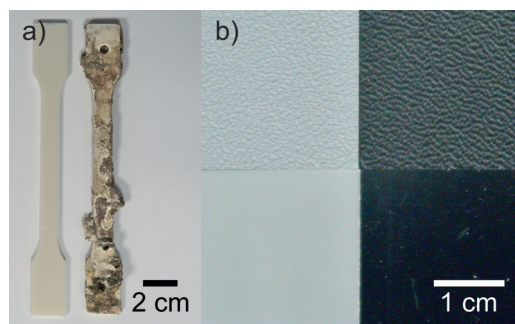


Figure 1. Sample overview. a) PHB plastic samples after fabrication and after exposure to marine environment, b) grained ASA and smooth ABS surface of ASA/ABS plastic sheets.

The scope of this work is to validate the μ CT-based method of topography characterization with a standard measurement, and to apply the μ CT-based method, to the best of the authors' knowledge for the first time, to the characterization of surfaces covered by a solid film, in this example the surface of a biodegradable PHB plastic covered by biofouling after exposure to marine environment.

2 Materials and Methods

2.1 Reference ASA/ABS Plastic Samples

As reference materials with uniform surface characteristics acrylonitrile styrene acrylate (ASA)/acrylonitrile butadiene styrene (ABS) plastic sheets (S-Polytec GmbH, Goch, Germany) produced by co-extrusion with a total thickness of 4 mm were used (Fig. 1b). One type of sample is colored gray throughout, the other type is colored black. Both types of reference samples feature one grained ASA surface and one smooth ABS surface. Samples with a size of approximately 20 mm \times 12 mm were cut out for measurement with optical profilometry as well as μ CT.

2.2 PHB Plastic Samples Exposed to Marine Environment

Polyhydroxybutyrate (PHB) is known to be a biodegradable polymer and often serves as positive control in degradation experiments [16–18]. PHB samples were fabricated of the material P209 (Biomer, Schwalbach, Germany) by injection molding. As sample geometry, the multipurpose test specimen type A according to EN ISO 3167:2014 [19] was used. The narrow parallel part of the test specimen, which was used for the topography characterization, has specified dimensions of 80 mm (length), 10 mm (width), and 4 mm (thickness). To study the degradation behavior under environmental conditions, PHB samples were exposed to pelagic conditions in the Southeast Asian ocean for several months by the Hydra Marine Sciences GmbH, i.e., the samples were suspended in the water column. As visible in Fig. 1a, the sample is covered by massive biofouling due to the exposure. The biofouling cannot be removed from the sample without damaging it, making it impossible to examine the sample surface and also the degree of disintegration using conventional methods.

2.3 μ CT Measurements

μ CT measurements were conducted on a CT-METRO device (Procon X-Ray GmbH, Sarstedt, Germany). The measurement parameters listed in Tab. 1 were applied.

For reconstruction of the volumetric data, the software CERA 6.0 (Siemens Healthcare GmbH, Erlangen, Germany) was used. Processing of the μ CT volume data was performed with the analysis software VGSTUDIO MAX 3.4 (Volume Graphics GmbH, Heidelberg, Germany).

For further processing, the plastic surface of the samples was determined by a locally adaptive surface determination based on gray value gradients. The PHB sample after fabrication shows a surface depression caused by shrinkage during fabrication. This means that the surface is not completely planar. To obtain data reproducing only the local surface

Table 1. μ CT measurement parameters of plastic samples.

Sample	X-ray tube voltage [kV]	X-ray tube current [μ A]	Voxel resolution [μ m]	Measuring time [min]
Reference ASA/ABS plastic samples	100	80	9.35	83
PHB samples after fabrication/after exposure to marine environment	80	60	5.61	319

topography and not the geometrical deviations, a geometry correction was performed on the μ CT data. This was achieved by fitting a free-form plane to the material surface and resampling the adjacent volume based on that. Subsequently, the surface area could be determined directly based on the local gray scale gradients. For the PHB sample after exposure to marine environment, the geometry correction was not necessary, because due to the strong roughening of the sample caused by degradation, shrinkage has a negligible influence on the surface geometry and roughness determination. Furthermore, due to the advanced disintegration process, the fitting of free-form surfaces would not be easily possible. In contrast, the massive film grown on this sample required segmentation of the plastic and bio-fouling before surface determination of the plastic could be performed. This was achieved by creating regions of interest based on appropriate gray value intervals and further manual refinement of the regions of interest. The region of interest describing the plastic was used as the basis for the locally adaptive surface determination. The ability to differentiate and analyze the two components separately is the major advantage of the μ CT method.

Regions of 10 mm \times 10 mm for the reference ASA/ABS samples and 6 mm \times 6 mm for the PHB samples of each surface were then converted to a grid-based surface mesh without any simplification, representing the determined surface as a point cloud. The individual points of the point cloud are described by x -, y -, and z -coordinates. Depending on the voxel resolution of the measurement and the topography, between approximately 14 000 and 108 000 points per square millimeter were generated. The highest number of points was generated for the rough surface of PHB sample after exposure to marine environment. While the examination of a larger area for the ASA/ABS samples was considered appropriate to obtain a representative reflection of the macro surface roughness of the grained surface, the smaller region size for the PHB samples was chosen to ensure sufficient distance to the edges of the sample to avoid falsification of the results.

2.4 Optical Profilometry Measurements

For optical profilometry (oPM), a 3D-Profilometer VR-3200 (Keyence Corporation, Osaka, Japan) was used. The

surface measurement relies on the fringe projection principle. For the macro measurement mode that was used, the measurement accuracy as specified by the manufacturer is $\pm 3 \mu\text{m}$ (height) and $\pm 5 \mu\text{m}$ (width). The whole sample surfaces of the reference ASA/ABS plastic samples were scanned. For further processing, the acquired 3D surfaces were exported as point clouds

consisting of x -, y -, and z -coordinates for each point. No simplification of the measured data was applied. The point clouds consisted of approximately 7000 points per square millimeter.

2.5 Determination of Surface Texture Properties

For analysis of the measured surface data, the open-source software Gwyddion 2.58 [20] was used. While developed for processing scanning probe microscopy data, it can be used for analysis of surface data from every kind of measurement. After import, the point cloud data obtained from oPM and μ CT measurements were rasterized to interpolate the data to a regular grid, i.e., a 2-dimensional image. The interpolation mode "Average" was used for this. With a three-point levelling function, the surface afterward was aligned horizontally. For the oPM measurements, the analysis region was restricted to an area of 10 mm \times 10 mm, corresponding to the regions extracted from the μ CT measurements of the reference ASA/ABS samples, respectively.

The specific surface area of a material is most often defined as the surface area per weight unit [21,22], but depending on application also a relation of the surface area to the bulk volume [23] or to the nominal area [24] can be useful. Because only the surface of a bulk material is characterized, in this work, the total surface area A_{total} is related to the nominal area A_{nominal} . Consequently, the specific surface area SSA is defined as:

$$\text{SSA} = \frac{A_{\text{total}}}{A_{\text{nominal}}} \quad (1)$$

For all reference measurements of the ASA/ABS samples, an area of 10 mm \times 10 mm is taken as the nominal area A_{nominal} . An area of 6 mm \times 6 mm is defined for the PHB samples after fabrication and after marine exposure to exclude influences of the edge regions. The corresponding total area A_{total} of the μ CT measurements is based on the surface determination by the CT analysis software, which uses local gray value gradients to determine the surface with an accuracy better than the μ CT voxel resolution [25]. For the oPM measurements, the surface area value from the statistical analysis of the software Gwyddion, which is computed by simple triangulation, is used as total area A_{total} .

For the 2-dimensional description of surface topographies, the common parameters S_q , S_z , S_{sk} , and S_{ku} are determined directly by the statistical analysis module of the software Gwyddion. The root mean square roughness S_q describes the standard deviation of the surface height distribution. The difference between the minimum and the maximum height value is described by the maximum height S_z . The skewness S_{sk} is a measure for the degree of symmetry of the height distribution. The kurtosis S_{ku} describes the sharpness of the height distribution. For mathematical definitions as well as further 2-dimensional roughness parameters, the reader is referred to Dong et al. [26–29].

3 Results and Discussion

3.1 Validation of μ CT-Based Topography Characterization

The internal structure of the ASA/ABS reference material can be seen in Fig. 2a based on the μ CT measurement. The gray and black ASA/ABS samples have comparable structural properties, which is why graphical representations are limited to the gray sample in the following. The samples are composed of a 3 mm-thick layer of ABS and a 1 mm-thick layer of ASA. Slightly different X-ray absorption properties of both materials result in different gray values in the μ CT images, allowing a distinction of the two components. Within the layers, the material is homogeneous and without defects. While the ABS layer features a smooth surface, the more weather resistant ASA is used for the grained surface, which is intended for visible surfaces. The maximum height deviation of the grained surface is about 150 μ m.

Fig. 3 compares the topography of the gray reference ASA/ABS sample as measured by oPM and μ CT. For the smooth surface, a grain in the top left leads to a different height scaling of the oPM measurement compared to the μ CT measurement. The grain is masked for the following evaluations. Apart from that, the surface features like the horizontal scratch and the slight pits are reproduced in a similar way by both measurements. The topography representations of the grained surface show a high similarity.

The surface texture properties as derived from oPM and μ CT measurements are listed in Tab. 2. The SSA value of the smooth surface is, as expected, close to $1 \text{ mm}^2 \text{ mm}^{-2}$ for all measurements. The SSA values of the grained surface is only slightly higher, showing that this parameter is not very sensitive for this kind of macro surface roughness. S_q values of maximum 3.67 μ m are within the range of expectation for the smooth surface of a finished plastic item [30]. The higher S_q values for the grained surface of

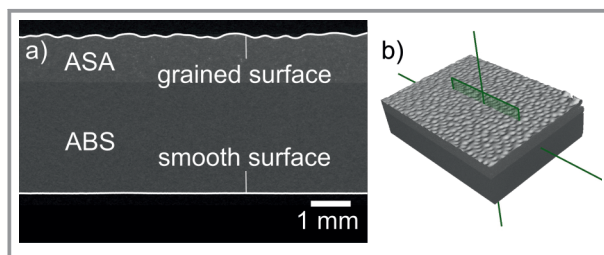


Figure 2. μ CT measurement of reference ASA/ABS plastic sample (gray). a) μ CT cross section with surface determination as white line, b) 3D rendering of μ CT measurement with indication of the cross section position.

maximum 32.51 μ m are in accordance with the intentionally produced surface texture. The maximum height S_z of the smooth surfaces depends primarily on local surface defects like scratches and is therefore not considered meaningful. For the grained surface, on the other hand, S_z values between 134 and 176 μ m reflect the intentionally produced surface texturing, as can also be traced from the CT cross section in Fig. 2a. The skewness values S_{sk} of smooth and grained surfaces are mainly close to zero, showing a homogeneous height distribution. As an exception, the CT measurement of the gray smooth surface gives a clearly negative value $S_{sk, \mu\text{CT}}$ of -1.53 , indicating significant depressions. The indentation at the upper edge in Fig. 3 is assumed to be the cause of this. Larger deviations are seen in the kurtosis values S_{ku} of the smooth surfaces, which vary between 2.16 and 8.16. While S_{ku} values below 3 indicate a height distribution that scatters more widely than a Gaussian distribution, values above 3 show a greater steepness of the height distribution than a Gaussian distribution [28]. With S_{ku} values between 2.16 and 2.30, a broadly scattered height distribution without domination of local extremes is obtained

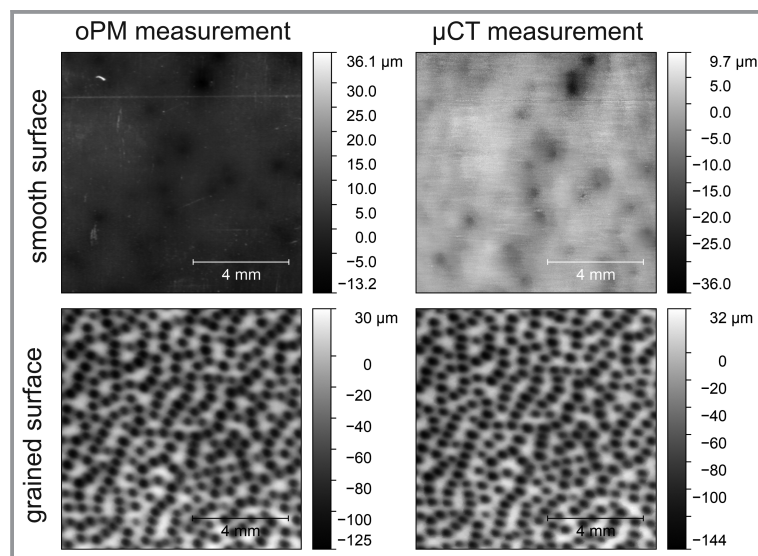


Figure 3. Topography of reference ASA/ABS plastic sample (gray) determined by oPM and μ CT measurement.

Table 2. Surface texture properties of reference ASA/ABS samples derived from oPM and μ CT measurements.

Sample	SSA_{oPM} [mm ² mm ⁻²]	$SSA_{\mu CT}$ [mm ² mm ⁻²]	$S_{q,oPM}$ [μ m]	$S_{q,\mu CT}$ [μ m]	$S_{z,oPM}$ [μ m]	$S_{z,\mu CT}$ [μ m]	$S_{sk,oPM}$ [-]	$S_{sk,\mu CT}$ [-]	$S_{ku,oPM}$ [-]	$S_{ku,\mu CT}$ [-]
Sample 1 (gray) smooth surface	1.00	1.02	2.40	3.67	28.73	45.69	-0.01	-1.53	4.36	8.16
Sample 1 (gray) grained surface	1.03	1.05	29.24	32.51	154.80	176.40	-0.04	-0.15	2.29	2.30
Sample 2 (black) smooth surface	1.00	1.01	1.36	2.45	28.83	29.43	-0.04	0.03	4.37	2.73
Sample 2 (black) grained surface	1.02	1.05	24.24	27.87	134.20	139.40	0.00	-0.12	2.19	2.16

for the grained surfaces. This is again expected for a surface with this kind of intentionally produced surface texturing.

Comparing both measurement methods, the SSA , S_q , and S_z values derived from the μ CT measurements are consistently higher than the values derived from the oPM measurements, but in a comparable range. For the grained surfaces, the deviations of SSA , S_q , and S_z are generally lower and do not exceed 13 %. Both S_{sk} and S_{ku} are sensitive to outliers [28]. While the S_{sk} and S_{ku} results for the grained surfaces correlate well between the two methods as well as the two samples, the high scatter in the S_{ku} values of the smooth surfaces indicates differences between oPM and μ CT in the reproduction of the sample topography. However, the general character of a low surface roughness is recognizable with both methods.

While the height measurement accuracy of oPM is specified as $\pm 3 \mu\text{m}$, the measurement accuracy of the μ CT measurements performed in the context of this work is not known. However, assuming that the surface area in CT measurements can be determined with an accuracy of up to 1/10 of the voxel resolution [25], a measurement accuracy of a comparable order of magnitude to the oPM measurement can be assumed for a voxel resolution of $9.35 \mu\text{m}$. Therefore, for the smooth surfaces with their very low roughness parameters, it can be assumed that equivalent results are obtained within the measurement accuracies of both methods that not fully reflect the topography of the smooth surfaces. Since the actual surface texture of the samples and the measurement accuracy of the μ CT measurement are not known, it is not possible to determine which method provides the more accurate results. Measurement inaccuracies of oPM could be due to shadowing effects on the grained surface, while the μ CT measurement could be influenced by measurement noise and CT-typical artifacts such as beam hardening or Feldkamp artifacts. It can be concluded that the μ CT method delivers comparable results to oPM and, therefore, is suitable for analyzing the surface

topography of plastic samples. However, a dimensional calibration and determination of the measurement accuracy of both methods would be recommended for future work to allow quantitative comparison of both methods.

3.2 Measurements of Samples Exposed to Marine Environment

The PHB sample after fabrication (Fig. 4) shows a homogeneous internal structure and a not strongly pronounced topography, similar to the smooth surface of the reference ASA/ABS sample. No cracks or pores are detectable. The surface depression owing to shrinkage during manufacture is visible. The values SSA , S_q , and S_z (Tab. 3) describing the surface texture are, as expected, nearly identical for both sides of the sample and slightly lower than for the smooth surface of the reference ASA/ABS samples, which reflects the low surface roughness of the sample surface. However, since the measurement accuracy is not known, this difference is not significant. The S_{sk} values of both surfaces are close to zero, again indicating a homogeneous height distribution. With S_{ku} values slightly larger than 3, the height distributions deviate marginally from a Gaussian distribution.

In comparison, the exposure of the PHB sample to marine conditions has caused significant changes in the sample due to material degradation. As visible in Figs. 1a, 5 and 6, biofouling has covered the whole sample and by this also the surface modification caused by biodegradation. The bio-

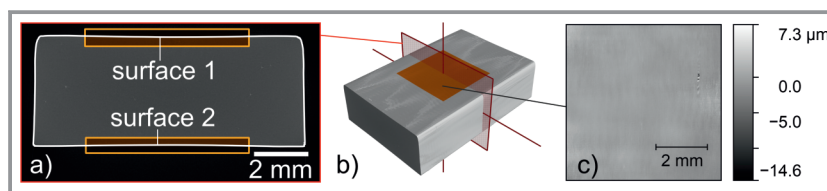


Figure 4. μ CT measurement of PHB sample after fabrication. a) μ CT cross section with surface determination as white line and with indication of analysis regions for topography characterization, b) 3D rendering of μ CT measurement with indication of the cross section position and analysis region surface 1, c) topography of surface 1 determined by μ CT measurement.

fouling is not uniform but is composed of a variation of microorganisms, differing in structure, size, and elemental composition. The dense layer on the left of Fig. 5c, e.g., has a similar gray level as the plastic. It can be assumed to have mainly an organic composition. The clearly lighter (high gray value level, i.e., a higher X-ray absorption) particulate growth on the right of Fig. 5c, in comparison, indicates a high inorganic content. Originating from the plastic surface, cracks have formed in the sample that extend to a depth of approx. 600 μm . Mainly on surface 1, reaching a depth of about 500 μm , the grow direction of the cracks changes to a partly parallel course related to the plastic surface, as can be seen in Fig. 5a. It is presumed that the transition from the outer amorphous to the inner region of the sample with a higher orientation of molecules in melt flow direction and a higher crystallinity [31–33] is causal for stopping the crack growth into the depth. These partially horizontal cracks inside the material cause a significantly broadened reproduction of the cracks in the topography visualizations in Fig. 5b and partially in Fig. 5d. The difference in the appearance of the cracks, as well as the difference in the structure of the biofouling between the two sides of the sample, could be due to variations in local environmental conditions, such as a predominant flow direction of the surrounding water.

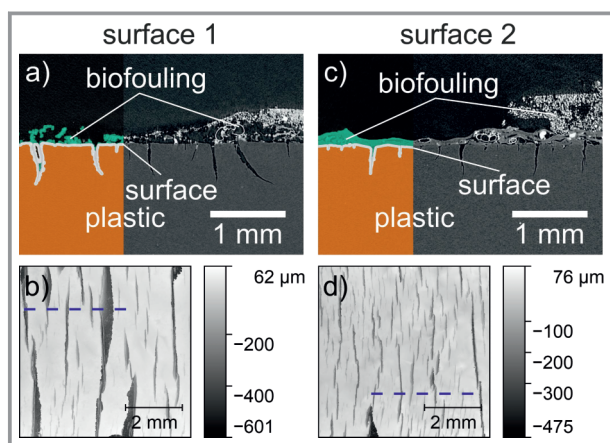


Figure 5. μCT measurement of PHB sample after exposure to marine conditions. a), c) μCT cross sections of surfaces 1 and 2 illustrating the segmentation of plastic and biofouling. b), d) Topography of surfaces 1 and 2 determined by μCT measurement. Dashed lines indicate the cross section positions of a) and c).

The biofouling can be differentiated from the plastic on the one hand by the gray value ranges, but also by the structural differences. The indication of the determined plastic surface in Figs. 5a and c as well as the color-coded 3D representation in Fig. 6 confirm that the μCT measurement allows to determine the plastic surface even below a solid film. In addition, tracing the cracks inside the material is easily achievable with μCT but would require a high preparative effort with other methods.

In comparison to the PHB sample after fabrication, the surface texture properties determined for the PHB sample

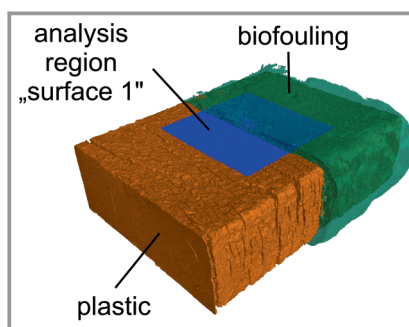


Figure 6. 3D rendering of μCT measurement of PHB sample after exposure to marine conditions illustrating the segmentation of plastic and biofouling. Rectangle indicates the analysis region surface 1.

after exposure to marine environment (Tab. 3) reflect the high increase of roughness of the surface due to disintegration events. A significant increase of SSA , S_q , and S_z before and after exposure demonstrates the degradation of the material. When comparing the surfaces, the roughness value S_q of surface 1 is about twice as high as of surface 2 after the exposure, while the specific surface area SSA of both surfaces is similar. The high S_q value for surface 1 results from the horizontal component of the cracks inside the material measured by μCT . As these crack components are located below the actual surface of the sample, they should not be considered as contributing to the actual surface roughness. Therefore, an interpretation of S_q values of these kind of samples must be done with caution. With values of 552 and 663 μm , the maximum height S_z correlates well with the observed depth of the cracks in the material. The S_{sk} values have developed distinctly into the negative, indicating the shift in the height distribution caused by the pronounced cracks. With S_{ku} values of up to 14, a pronounced deviation of the height distribution from a Gaussian normal distribution is indicated, which is characterized by the cracks as sig-

Table 3. Surface texture properties of PHB samples after fabrication and after exposure to marine environment derived from μCT measurements.

Sample	$SSA_{\mu\text{CT}}$ [$\text{mm}^2\text{mm}^{-2}$]	$S_{q,\mu\text{CT}}$ [μm]	$S_{z,\mu\text{CT}}$ [μm]	$S_{sk,\mu\text{CT}}$ [-]	$S_{ku,\mu\text{CT}}$ [-]
PHB sample after fabrication – surface 1	1.01	0.41	11.84	0.32	4.85
PHB sample after fabrication – surface 2	1.01	0.61	6.18	-0.14	4.50
PHB sample after exposure – surface 1	2.53	106.1	662.9	-2.18	6.73
PHB sample after exposure – surface 2	2.44	57.09	551.5	-2.94	14.00

nificant outliers. The large difference between the S_{ku} values of surfaces 1 and 2 is probably due to the fact that surface 2 has a much more uniform pattern of cracks, causing a higher kurtosis.

An adjustment of the evaluation methodology towards a differentiated approach of surficial structures and in-depth cracks would enable even greater informative value. The microroughness of the outer surface could be specifically relevant for the early settlement of microorganisms, which creates the basis for further biological degradation processes. A quantity that specifically describes the extent of cracking, on the other hand, could represent the preliminary stage of disintegration into macroscopic fragments.

In contrast to S_q , SSA reflects the surface area available for, e.g., degradation reactions within the nominal area under investigation and, thus, by definition, includes horizontal crack components within the sample as long as they are associated with the surface. The significant increase of SSA in comparison to the sample after fabrication reflects the advanced stage of the fragmentation process.

The potential and feasibility of investigating the degradation behavior and, in particular, the changes in the surface properties of plastics by means of μ CT were demonstrated. For systematic statements on the degradation processes in marine environments, the investigation of further samples would be required, but this was not performed at this stage of exemplary demonstration of the methodology due to the high effort required for the exposition and measurement of samples.

The ability to measure the surface texture properties of plastic samples even when covered by biofouling could be also used, e.g., to analyze the effect of different surface roughnesses on the settlement and further growth of microorganisms and their effect on the fragmentation and degradation process. In principle, the same sample could be examined repeatedly to map the temporal progression.

4 Conclusions

The micro-computed tomography is a versatile method for microstructural studies in a wide variety of scientific disciplines. In this work, the applicability of the method for the topography characterization of plastic materials was demonstrated. Reference measurements on plastic samples with uniform structure, performed comparatively with μ CT and conventional optical profilometry, allowed us to validate the methodology for determining surface properties like S_q , S_z , and SSA, confirming the results previously reported for the characterization of additively manufactured components [6–10], especially for microstructured surfaces. However, measurements on calibrated instruments with known measurement accuracy would be recommended for the future to quantitatively compare the actual measurement accuracy of oPM and μ CT and to define the work area of the method.

Building on this, it was shown for the first time that it is also possible to use the μ CT-based method to characterize a surface that is completely covered and therefore hidden by a solid film. This was exemplified by a plastic surface that was covered with heavy biofouling due to marine exposure. In addition to the detailed description of the surface topography, μ CT also allows the determination of degradation levels or biofouling coverage for such samples. However, the application is not limited to the study of marine degradability of plastics. Since the μ CT method is largely material-independent (as long as the material is transparent to X-rays), it can be applied to a wide variety of scenarios in which the surface to be investigated is covered by a film or is generally inaccessible. This could be, e.g., materials susceptible to corrosion with applied protective coatings as well as catalytically active surfaces prone to inactivating films. In medical research, this could be relevant for implant materials on which tissue grows. In contrast, conventional methods are generally preferable for freely accessible surfaces due to the comparatively high measurement effort of μ CT.

Further development of the μ CT method would require measurements of samples with known surface texture properties to determine the measurement errors as a function of surface texture, material, and μ CT measurement parameters. Additionally, the evaluation procedure could be further adapted to obtain metrics that are meaningful for the research question, especially for complex surface structures. For the investigation of the degradation behavior of plastics, e.g., this could mean differentiating between the microroughness of the outer surface and the progress of crack growth inside the material.

The financial support for this research by the BMEL (German Federal Ministry of Food and Agriculture, Funding code: 22028618, project name “MabiKu”), implemented by the FNR (Fachagentur Nachwachsende Rohstoffe e.V., Germany), is gratefully acknowledged. We would further like to thank Sinan Yarcu (Leibniz University Hannover, Institute of Forming Technology and Machines, Germany) for carrying out profilometer measurements and Miriam Weber as well as Christian Lott (HYDRA Marine Sciences GmbH, Germany) for providing a PHB sample that was exposed to marine conditions. Open access funding enabled and organized by Projekt DEAL.

Symbols used

A_{nominal}	[mm ²]	nominal area
A_{total}	[mm ²]	total surface area
S_{ku}	[-]	kurtosis of topography height distribution

S_{sk}	[-]	skewness of topography height distribution
SSA	[mm ² mm ⁻²]	specific surface area
S_q	[μm]	root mean square roughness
S_z	[μm]	maximum height

Sub- and superscripts

oPM	value based on optical profilometry measurement
μCT	value based on micro-CT measurement

Abbreviations

ABS	acrylonitrile butadiene styrene
ASA	acrylonitrile styrene acrylate
CT	computed tomography
oPM	optical profilometry
PHB	polyhydroxybutyrate

References

- [1] R. Leach, *Optical Measurement of Surface Topography*, Springer, Berlin **2011**.
- [2] DIN EN ISO 25178-6:2010, *Geometrische Produktspezifikation (GPS) – Oberflächenbeschaffenheit: Flächenhaft – Teil 6: Klassifizierung von Methoden zur Messung der Oberflächenbeschaffenheit (ISO 25178-6:2010)*, Beuth, Berlin **2010**.
- [3] P. J. Withers, C. Bouman, S. Carmignato, V. Cnudde, D. Grimaldi, C. K. Hagen, E. Maire, M. Manley, A. Du Plessis, S. R. Stock, *Nat. Rev. Methods Primers* **2021**, *1* (1), 18. DOI: <https://doi.org/10.1038/s43586-021-00015-4>
- [4] L. Vásárhelyi, Z. Kónya, Á. Kukovecz, R. Vajtai, *Mater. Today Adv.* **2020**, *8*, 100084. DOI: <https://doi.org/10.1016/j.mtadv.2020.100084>
- [5] L. de Chiffre, S. Carmignato, J.-P. Kruth, R. Schmitt, A. Weckenmann, *CIRP Ann.* **2014**, *63* (2), 655–677. DOI: <https://doi.org/10.1016/j.cirp.2014.05.011>
- [6] G. Kerckhofs, G. Pyka, M. Moesen, J. Schrooten, M. Wevers, in *Proc. of Conf. on Industrial Computed Tomography (ICT) 2012* (Ed: J. Kastner), Shaker, Aachen **2012**.
- [7] C. G. Klingaa, M. K. Bjerre, S. Baier, L. de Chiffre, S. Mohanty, J. H. Hattel, in *9th Conf. on Industrial Computed Tomography (iCT) 2019*, NDT.net, Bad Breisig, Germany **2019**.
- [8] A. Du Plessis, S. G. Le Roux, J. Waller, P. Sperling, N. Achilles, A. Beerlink, J.-F. Métayer, M. Sinico, G. Probst, W. Dewulf, F. Bittner, H.-J. Endres, M. Willner, Á. Drégelyi-Kiss, T. Zikmund, J. Laznovsky, J. Kaiser, P. Pinter, S. Dietrich, E. Lopez, O. Fitzek, P. Konrad, *Addit. Manuf.* **2019**, *30*, 100837. DOI: <https://doi.org/10.1016/j.addma.2019.100837>
- [9] A. Du Plessis, P. Sperling, A. Beerlink, O. Kruger, L. Tshabalala, S. Hoosain, S. G. Le Roux, *MethodsX* **2018**, *5*, 1111–1116. DOI: <https://doi.org/10.1016/j.mex.2018.09.004>
- [10] V. Aloisi, S. Carmignato, *Case Stud. Nondestr. Test. Eval.* **2016**, *6*, 104–110. DOI: <https://doi.org/10.1016/j.csndt.2016.05.005>
- [11] D. K. A. Barnes, F. Galgani, R. C. Thompson, M. Barlaz, *Philos. Trans. R. Soc. London, Ser. B* **2009**, *364* (1526), 1985–1998. DOI: <https://doi.org/10.1098/rstb.2008.0205>
- [12] C. P. Ward, C. M. Reddy, *PNAS* **2020**, *117* (26), 14618–14621. DOI: <https://doi.org/10.1073/pnas.2008009117>
- [13] A. Göpferich, *Biomaterials* **1996**, *17* (2), 103–114. DOI: [https://doi.org/10.1016/0142-9612\(96\)85755-3](https://doi.org/10.1016/0142-9612(96)85755-3)
- [14] A. L. Andradý, *J. Macromol. Sci., Polym. Rev.* **1994**, *34* (1), 25–76. DOI: <https://doi.org/10.1080/15321799408009632>
- [15] T. P. Haider, C. Völker, J. Kramm, K. Landfester, F. R. Wurm, *Angew. Chem., Int. Ed.* **2019**, *58* (1), 50–62. DOI: <https://doi.org/10.1002/anie.201805766>
- [16] C. Lott, A. Eich, D. Makarow, B. Unger, M. van Eekert, E. Schuman, M. S. Reinach, M. T. Lasut, M. Weber, *Front. Mar. Sci.* **2021**, *8*, 662074. DOI: <https://doi.org/10.3389/fmars.2021.662074>
- [17] A. Eich, M. Weber, C. Lott, *PeerJ* **2021**, *9*, e11981. DOI: <https://doi.org/10.7717/peerj.11981>
- [18] J. Mergaert, A. Wouters, C. Anderson, J. Swings, *Can. J. Microbiol.* **1995**, *41* (13), 154–159. DOI: <https://doi.org/10.1139/m95-182>
- [19] DIN EN ISO 3167:2014, *Kunststoffe – Vielzweckprobekörper (ISO 3167:2014)*, Beuth, Berlin **2014**.
- [20] D. Nečas, P. Klapetek, *Cent. Eur. J. Phys.* **2012**, *10* (1), 181–188. DOI: <https://doi.org/10.2478/s11534-011-0096-2>
- [21] K. D. Pennell, in *Reference Module in Earth Systems and Environmental Sciences*, Elsevier, Amsterdam **2016**.
- [22] J. E. Funk, D. R. Dinger, in *Predictive Process Control of Crowded Particulate Suspensions* (Eds: J. E. Funk, D. R. Dinger), Springer, Boston, MA **1994**.
- [23] R. M. Tiggelaar, V. Verdoold, H. Eghbali, G. Desmet, J. G. E. Gardeniens, *Lab Chip* **2009**, *9* (3), 456–463. DOI: <https://doi.org/10.1039/B812301B>
- [24] F. Bittner, T. Oekermann, M. Wark, *Materials* **2018**, *11* (2), 232. DOI: <https://doi.org/10.3390/ma11020232>
- [25] S. Rieth-Hoerst, C. Reinhart, T. Günther, T. Dierig, J. Fieres, in *11th Eur. Conf. on Non-Destructive Testing (ECNDT 2014)*, NDT.net, Bad Breisig, Germany **2014**.
- [26] W. P. Dong, P. J. Sullivan, K. J. Stout, *Wear* **1992**, *159* (2), 161–171. DOI: [https://doi.org/10.1016/0043-1648\(92\)90299-N](https://doi.org/10.1016/0043-1648(92)90299-N)
- [27] W. P. Dong, P. J. Sullivan, K. J. Stout, *Wear* **1993**, *167* (1), 9–21. DOI: [https://doi.org/10.1016/0043-1648\(93\)90050-V](https://doi.org/10.1016/0043-1648(93)90050-V)
- [28] W. P. Dong, P. J. Sullivan, K. J. Stout, *Wear* **1994**, *178* (1–2), 29–43. DOI: [https://doi.org/10.1016/0043-1648\(94\)90127-9](https://doi.org/10.1016/0043-1648(94)90127-9)
- [29] W. P. Dong, P. J. Sullivan, K. J. Stout, *Wear* **1994**, *178* (1–2), 45–60. DOI: [https://doi.org/10.1016/0043-1648\(94\)90128-7](https://doi.org/10.1016/0043-1648(94)90128-7)
- [30] www.myplasticmold.com/surface-roughness.html (Accessed on September 03, 2021)
- [31] T. A. Osswald, E. Baur, N. Rudolph, *Plastics Handbook: The Resource for Plastics Engineers*, 5th ed., Hanser, München **2017**.
- [32] K. Albrecht, E. Baur, H.-J. Endres, R. Gente, N. Graupner, M. Koch, M. Neudecker, T. Osswald, P. Schmidtke, S. Wartzack, K. Weibelhaus, J. Müssig, *Composites, Part A* **2017**, *95*, 54–64. DOI: <https://doi.org/10.1016/j.compositesa.2016.12.022>
- [33] L. Veltmaat, H.-J. Endres, F. Bittner, *Z. Kunststofftech.* **2021**, *17* (3), 129–151. DOI: <https://doi.org/10.3139/O999.01032021>